Editor's Choice
Microscopy, 2022, **71(2)**, 93–97
DOI: https://doi.org/10.1093/jmicro/dfab054
Advance Access Publication Date: 3 December 2021
Article

MICROSCOPY

Lorentz scanning electron/ion microscopy

Ken Harada[1,*], Keiko Shimada[1] and Yoshio Takahashi[2]

[1]CEMS, RIKEN (Institute of Physical and Chemical Research), Hatoyama, Saitama 350-0395, Japan
[2]Research and Development Group, Hitachi, Ltd., Hatoyama, Saitama 350-0395, Japan
*To whom correspondence should be addressed. E-mail: kharada@riken.jp

Abstract

We have developed an observation and measurement method for spatial electromagnetic fields by using scanning electron/ion microscopes, combined with electron holography reconstruction technique. A cross-grating was installed below the specimen, and the specimens were observed under the infocus condition, and the grating was simultaneously observed under the defocus condition. Electromagnetic fields around the specimen were estimated from grating-image distortions. This method is effective for low and middle magnification and resolution ranges; furthermore, this method can in principle be realizable in any electron/ion beam instruments because it is based on the Lorentz force model for charged particle beams.

Key words: Lorentz force model, charged particle beams, spatial electromagnetic fields, grating image, reconstruction technique, electron holography

Introduction

Scanning electron microscope (SEM) is one of the most widely used electron beam devices, for example, in materials science fields, semiconductor fields and medical and bio-science fields. This is because SEM can not only observe specimen shapes, structures and surface conditions but also analyse material elements at and around the specimen surfaces by using energy-dispersive X-ray spectroscopy. Furthermore, SEM is relatively easy to operate and the interpretation of obtained SEM images can be done intuitively.

However, sometimes, SEM images show interesting characteristics, for example, heavily distorted background lines around a piece of copper as shown in Fig. 1. These lines are due to inside structures of the SEM column. Here, the specimen itself was observed under the infocus condition, while the background was observed under the defocus condition, resulting in heavily distorted images. Although it has been known that such defocused and distorted images contain information on spatial electromagnetic fields around the specimen, using these images for electromagnetic field measurement has not been fully discussed yet.

Several pioneering studies for measuring magnetic fields by electron beam deflection using SEM [1–3] did not show specimen images together with field distributions. In the present paper, we report the development of a visualization method for observing both electromagnetic fields and specimen images under the infocus condition. The phase reconstruction techniques and phase analysis techniques of electron holography were added to this method.

Theoretical

The image distortion of gratings under the defocus condition can be explained by the interaction between charged particle beams and electromagnetic fields, such as Lorentz force given by

$$\boldsymbol{F}(\boldsymbol{r}) = -e\left(\boldsymbol{E}(\boldsymbol{r}) + \boldsymbol{v} \times \boldsymbol{B}(\boldsymbol{r})\right) \tag{1}$$

where $\boldsymbol{F}$ is Lorentz force, including the Coulomb force, $-e$ is electron charge, $\boldsymbol{v}$ is electron velocity, $\boldsymbol{E}$ is electric field, $\boldsymbol{B}$ is magnetic flux density and $\boldsymbol{r}$ is position vector [4–6]. Electron beam deflections are discussed in the uniform and constant field approximation [7] using Fig. 2. For simplicity, electric fields and magnetic fields are discussed separately, assuming that the deflection is only in the x-direction. This method can be applied to Ga^+ ion beam case to be described later.

Electric field

The deflection angle α is given by the ratio of momentum of deflected electron, $eE \times l/v$, to the that of incident electron, mv,

$$\alpha = \frac{eE \times \frac{l}{v}}{mv} = \frac{eEl}{mv^2} = \frac{El}{2V_0} \tag{2}$$

where l is the vertical region of electric/magnetic field and V_0 is acceleration voltage. The angle α can also be expressed in terms of the distortion Δx and defocus distance Δf as

$$\alpha = \frac{\Delta x}{\Delta f} \tag{3}$$

Received 3 November 2021; Revised 28 November 2021; Editorial Decision 30 November 2021; Accepted 1 December 2021

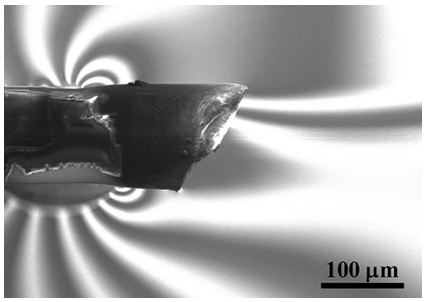

Fig. 1. SEM image with largely distorted background lines.

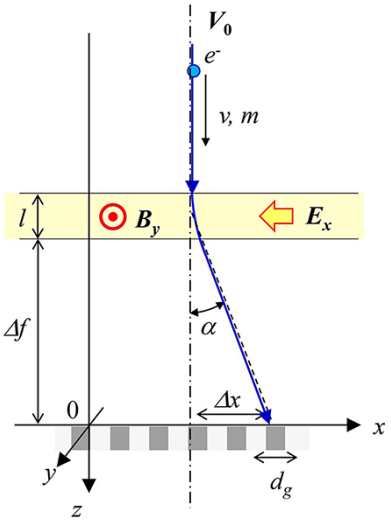

Fig. 2. Schematics of particle beam deflection in the uniform and constant field model.

When the grating distortion Δx is expressed by a phase of the grating, $\eta(x) = 2\pi\Delta x/d_g$, with d_g being the grating space, then electric field $E(x)$ is expressed by

$$E(x) = \frac{2V_0}{l}\alpha = \frac{2V_0}{2\pi}\frac{d_g}{l\Delta f}\eta(x) \tag{4}$$

The equi-phase contour image $\cos[\eta(x)]$, corresponding to an equi-electric field image, is given by

$$\cos[\eta(x)] = \cos\left[\frac{2\pi}{2V_0}\frac{l\Delta f}{d_g}E(x)\right] \tag{5}$$

and an equi-electric field E_{eq} between the contour fringes is defined by putting $\eta(x) = 2\pi$

$$E_{eq} = \frac{2V_0}{l}\frac{d_g}{\Delta f} \tag{6}$$

Electric field has the same scalar value for E_{eq} between the contour fringes.

In experimental observations discussed later, projected fields are given by either $E(x)\times l$ or $E_{eq}\times l$ within the present approximation.

To compare the results with electron holography observations results [8], the deflection angle α is expressed by the momentum ratio written in terms of potentials as

$$\alpha = \sqrt{\frac{V_x}{V_0}} \tag{7}$$

where V_x is the electron deflecting potential in the x direction. Then, the distribution of $V_x(x)$ is given by

$$V_x(x) = \alpha^2 V_0 = \frac{V_0}{(2\pi)^2}\frac{{d_g}^2}{(\Delta f)^2}\eta(x)^2 \tag{8}$$

The equi-potential contour image $\cos[\eta(x)]$ and an equi-potential V_{xeq} between the contour fringes can be written as

$$\cos[\eta(x)] = \cos\left[2\pi\frac{\Delta f}{d_g}\sqrt{\frac{V_x(x)}{V_0}}\right] \tag{9}$$

$$V_{xeq} = \frac{{d_g}^2}{\Delta f^2}V_0 \tag{10}$$

In the two-dimensional analysis, the electric field distribution $E(x, y)$ is expressed by

$$|E(x,y)| = \sqrt{E(x)^2 + E(y)^2} = \frac{2V_0}{2\pi}\frac{d_g}{l\Delta f}\sqrt{\eta(x)^2 + \eta(y)^2} \tag{11}$$

$$E(x) = \tfrac{2V_0}{2\pi}\tfrac{d_g}{l\Delta f}\eta(x),\ E(y) = \tfrac{2V_0}{2\pi}\tfrac{d_g}{l\Delta f}\eta(y).$$

Magnetic field

For magnetic field analyses, the deflection angle α is expressed by

$$\alpha = \frac{eBl}{mv} = \frac{e}{h}B_y l\lambda \tag{12}$$

where h is Plank's constant, λ is wavelength, and B_y is magnetic flux density in the y direction.

Then $B_y(x)$ is expressed by

$$B_y(x) = \frac{h}{e}\frac{\alpha}{l\lambda} = \frac{1}{2\pi}\frac{h}{e}\frac{d_g}{l\lambda\Delta f}\eta(x) = \frac{1}{2\pi\lambda}\Phi_0\frac{d_g}{l\Delta f}\eta(x) \tag{13}$$

where Φ_0 is the unit magnetic flux constant $\Phi_0 = h/e = 4.15\times10^{-15}$ Wb [4,5,7].

In the contour image of $\cos[\eta(x)]$, an equi-magnetic flux density B_{yeq} between the contour fringes is defined by putting $\eta(x) = 2\pi$

$$B_{yeq} = \frac{\Phi_0}{\lambda}\frac{d_g}{l\Delta f} \tag{14}$$

Magnetic field along the y direction has the same scalar value for B_{yeq} between the contour fringes.

In the experiments, we observe the projected magnetic flux density given by either $B_y(x)\times l$ from Eq. (13) or $B_{yeq}\times l$ from Eq. (14).

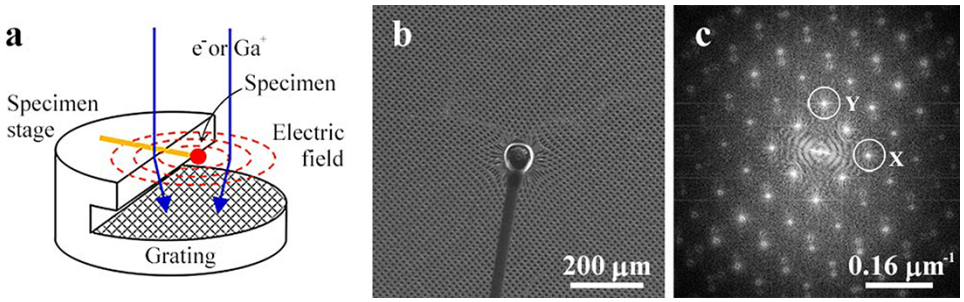

Fig. 3. (a) Experimental setup; (b) 15-kV SEM image for electric field observation; (c) fast Fourier transformed pattern of (b).

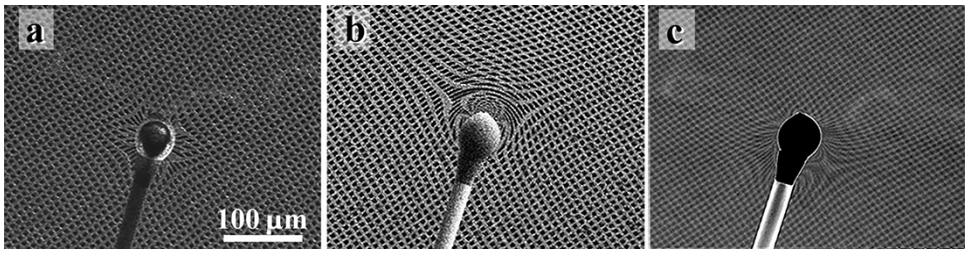

Fig. 4. (a) SEM image (shrink type) for 5-kV electron beams with negative charge accumulation; (b) SEM image (expansion type) for 2-kV electron beams with positive charge accumulation; (c) SIM image (shrink type) for 5-kV Ga^+ ion beam with positive charge accumulation.

To compare these results with electron holography observation results [8], we use the magnetic flux Φ_y between the contours given by

$$\Phi_y = B_{yeq} d_g l = \frac{{d_g}^2}{\lambda \Delta f} \Phi_0 \tag{15}$$

In the two-dimensional analysis, magnetic flux density distribution $|B(x, y)|$ is expressed by

$$|B(x,y)| = \frac{\Phi_0}{2\pi\lambda} \frac{d_g}{l\Delta f} \sqrt{\eta_x(x,y)^2 + \eta_y(x,y)^2} \tag{16}$$

where $\eta_x(x, y)$ is two-dimensional distribution of distortion in the x direction, and $\eta_y(x, y)$ is two-dimensional distribution of distortion in the y direction.

Experimental

Figure 3a shows an experimental setup of the specimen stage and cross-grating. The specimen for electric field observation was an epoxy resin attached to the tip of a copper wire. The grating was made up of a copper cross-grid with a period of 12.7 μm. The distance between the specimen position and the grating was 5 mm. Figure 3b shows an SEM image at the acceleration voltage of 15 kV ($\lambda = 9.93$ pm), having grating images distorted by induced electric fields through beam irradiation. Figure 3c shows a fast Fourier transformed pattern of (b). Two orthogonal Fourier spots in circles A and B in (c) were used for the reconstruction to be discussed later.

Figure 4 shows scanning electron micrographs (SEM images) in (a) and (b), and a scanning ion micrograph (SIM image) using Ga^+ in (c), obtained by using a focused ion beam (FIB) instrument NB-5000 (Hitachi High Tech). We used the same specimen for Fig. 3b. The amount of charge at the epoxy resin, which generated the electric fields, changed substantially depending on the amount of irradiation beam currents, irradiation time and acceleration voltage. The distortion profile of the grating images depended on the polarity of the charge up.

The deflection in the positive x-direction in Fig. 2 leads to shrink-type distortions, while the deflection in the negative x-direction leads to expansion-type distortions. The shrink-type distortion in Fig. 4a by 5-kV electron beam ($\lambda = 17.3$ pm) shows accumulated negative charges at the epoxy resin. The expansion-type distortion in Fig. 4b by 2-kV electron beam ($\lambda = 27.4$ pm) shows the accumulation of positive charges. The shrink-type distortion in Fig. 4c by 5-kV Ga^+ ion beam ($\lambda = 0.0486$ pm) shows accumulated positive charges. We note that the charging polarities in (a) and (c) show opposite characteristics from ordinarily considered phenomena in high-speed charged particle beams, indicating the complexity of charge accumulation phenomena. We note that the question as to why both positive and negative charging was obtained remains to be investigated. However, the different experimental conditions should be considered in the analysis. For Figs. 4a and b, charging was related to the difference of acceleration voltage of irradiating electrons, while for Figs. 4a and c, charging was related to the difference of polarities of the irradiated particles.

The distortion of the grating image can be numerically estimated through the reconstruction method of electron holography using two orthogonal Fourier spots X and Y shown in Fig. 3c. When we use these spots as phase distribution $|\eta(x, y)|$ defined by

$$|\eta(x,y)| = \sqrt{\eta_x(x,y)^2 + \eta_y(x,y)^2} \tag{17}$$

then electric field $|E(x, y)|$ and magnetic flux density $|B(x, y)|$ can be written as

$$|E(x,y)| = \frac{2V_0}{2\pi} \frac{d_g}{l\Delta f} |\eta(x,y)| \tag{18}$$

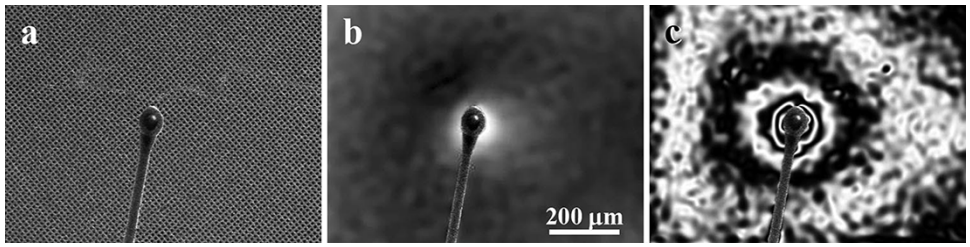

Fig. 5. (a) 2-kV SEM image of epoxy resin with distorted grating image; (b) reconstructed distortion image from the of distorted image in (a); (c) contour map of projected electric field from (b).

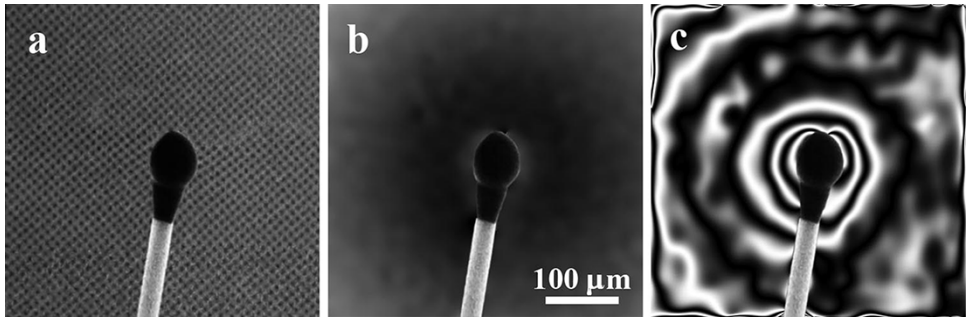

Fig. 6. (a) 10-kV SIM image of epoxy resin with distorted grating image; (b) reconstructed distortion image from the distorted image in (a); (c) contour map of projected electric field from (b).

$$
\begin{aligned}
|B(x,y)| &= \sqrt{B_y(x,y)^2 + B_{-x}(x,y)^2} \\
&= \frac{\Phi_0}{2\pi\lambda}\frac{d_g}{l\Delta f}\sqrt{\eta_x(x,y)^2 + \eta_y(x,y)^2} \\
&= \frac{\Phi_0}{2\pi\lambda}\frac{d_g}{l\Delta f}|\eta(x,y)|
\end{aligned}
\tag{19}
$$

We note that all these equations written above do not depend on the particle charge or mass because the developed method is in principle applicable to any particle beam instruments.

Results and discussion

We applied the developed method to analyse electric fields and magnetic flux densities using electrons and Ga^+ ions.

Electric field

Figure 5a shows a 2-kV SEM ($\lambda = 27.4$ pm) image of the epoxy resin with distorted grating image behind the resin; Fig. 5b shows a reconstructed distortion image from the distorted image in Fig. 5a through Eq. (17) using holography reconstruction algorism; and Fig. 5c shows $\cos|\eta(x, y)|$ image as an equi-electric field contour map obtained from Fig. 5b. Figure 5b and c are composite images of the infocused epoxy resin. With the phase amplification of 5, a projected electric field $E_{eq} \times l$ between contours in Fig. 5c is about 2.0 V using Eq. (6). Here, the projected electric field defined by equi-electric field E_{eq} times field region l has a dimension of electric potential V. When the resin thickness at the tip of Cu wire was reduced to that of the side of the wire, the electric field distribution becomes symmetrical.

Figure 6a shows an SIM ($\lambda = 0.0344$ pm) image of the epoxy resin and grating image behind the resin for 10-kV Ga+ ion beam; Fig. 6b shows a reconstructed distortion image from the distorted image in Figs. 6a and c shows an equi-electric-field contour map obtained from (b). Figure 6b and c are composite images of infocused epoxy resin. With the phase amplification of 5, a projected electric field $E_{eq} \times l$ between contours in Fig. 6c is about 10.2 V. The quantity of charge accumulation depends on the acceleration voltage of the beam. From these experiments, we find that higher acceleration voltage leads to a larger accumulation of charges on the resin. We think that this relation depends on acceleration voltage of electrons, penetration depth and ionization process of the resin. However, the detailed mechanisms remain to be investigated.

Magnetic flux density

For magnetic flux density observation, we used commercially available ferrite magnets as specimen. A small bar magnet with 100 µm length was prepared by the FIB instrument, and twin bar magnets were lined up to strengthen spatial magnetic fields. To decrease leakage magnetic fields in the pole-piece position in the FIB instrument, the specimen stage was lowered by 17 mm from the normal position.

Figure 7a shows a 5-kV SEM ($\lambda = 17.3$ pm) image of the twin bar magnets and grating image behind the magnets; Fig. 7b shows the reconstructed distortion image from the distorted image in Figs. 7a and c shows a contour map of equi-magnetic flux density calculated from Fig. 7b. Figure 7b and c are composite images of the magnets shown in Fig. 7a. Phase amplification in (c) is 13 calculated using Eq. (14), corresponding to projected magnetic flux density $B_{eq} \times l = 143$ $\Phi_0/d_g = 4.7 \times 10^{-8}$ Wb/m between contours. Here, the projected magnetic field density defined by the equi-magnetic flux

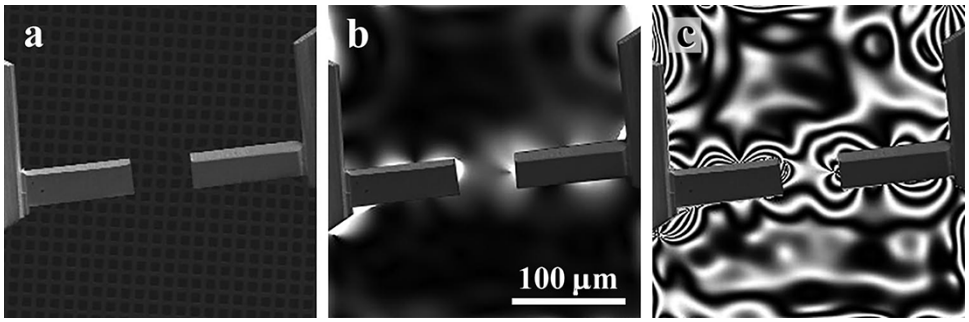

Fig. 7. (a) 5-kV SEM image of twin bar magnets with distorted grating image; (b) reconstructed distortion image from the distorted image in (a); (c) contour map of projected magnetic flux density from (b).

density B_{eq} times field region l has a dimension of magnetic flux by distance, Wb/m. The twin magnets were arranged in the line-up fashion; however, the number of contours of equi-magnetic flux density was smaller than the expected value, and some contours closed at the surface of the magnets, indicating that this 100-mm-long bar magnet has multi-domain structures.

Spatial magnetic flux density could not be observed clearly with 5-kV Ga^+ ion beam, probably because the Ga^+ ion mass was too large to bend grid images with sufficient distortions.

Conclusion

We have developed a method for the observation and measurement of spatial electromagnetic fields by using scanning electron/ion microscopes, together with the electron holography reconstruction techniques.

By placing the cross-grating under the specimen, we observed the specimen with electromagnetic fields under the infocus condition, while simultaneously observing the gratings under the defocus conditions, such as Lorentz condition. The electromagnetic fields were measured in terms of distortions of grating images qualitatively and quantitatively. The grating was used for detecting the deflection angles of the electron/ion beams.

Since this method depends only on the Lorentz force model for charged particle beams, it can be realized using any electron/ion beam instruments without requiring high-end holography electron microscopes. In addition, this method can be applied to low or middle magnification and resolution conditions. We note that this method requires small grids and regular array gratings for high-resolution and high-magnification observations.

This method can also be used in transmission electron microscopes in the conventional mode. In the near future, we intend to extend this method to measurements of wide-area observations of electromagnetic fields where electron holography is not applicable. Furthermore, the schlieren method [9,10] will be incorporated in the analysis.

Funding

This work was supported by JSPS KAKENHI, Grant-in-Aid for Scientific Research, Grant Number 20K20555.

Acknowledgements

We are grateful to Dr. Y. A. Ono of RIKEN and Dr. H. Shinada and Dr. T. Kohashi of Hitachi, Ltd. for valuable discussions, Mr. N. Moriya of Hitachi, Ltd. for technical support for developing the specimen stage, and Mr. Y. Ichinosawa of Optnics Precision Co., Ltd. for technical support on the gratings. We thank Prof. S. Mori, Prof. Y. Ishii, and Dr. H. Nakajima of Osaka Prefecture University for evaluation of the ferrite magnets.

References

1. Thornley R F M and Hutchison J D (1968) Magnetic field measurements in the scanning electron microscope. *Appl. Phys. Lett.* 13: 249–250.
2. Ishiba T and Suzuki H (1974) Measurements of magnetic field of magnetic recording head by scanning electron microscope. *Jpn. J. Appl. Phys* 13: 457–462.
3. Elsbrock J B and Balk L J (1984) Profiling of micromagnetic stray fields in front of magnetic recording media and heads by means of a SEM. *IEEE Trans. Mag.* 20: 865–868.
4. Tonomura A (1999) *Electron Holography*. 2nd edn (Springer, Heidelberg).
5. Tonomura A (1987) Applications of electron holography. *Rev. Mod. Phys.* 59: 639–669.
6. Harada K (2015) Lorentz microsopy. *Kenbikyo* 50: 118–125. (in Japanese).
7. Harada K, Endo J, Osakabe N, and Tonomura A (2008) Direction-free magnetic field application system. *e-J. Surf. Sci. Nanotech.* 6: 29–34.
8. Harada K (2021) Interference and Interferometry in electron holography. *Microscopy* 70: 3–16.
9. Harada K, Kawaguchi A, Kotani A, Fujibayashi Y, Shimada K, and Mori S (2019) Hollow-cone Foucault imaging method. *Appl. Phys. Express* 12: 1–4.
10. Harada K, Mori S, and Takahashi Y (2021) Schlieren imaging of spatial magnetic fields by hollow-cone illumination. *Microsc. Microanal.* 27: 2318–2319.